The Phoenix Deep Survey: The star-formation rates and the stellar masses of EROs

A. Georgakakis[1]⋆, A. M. Hopkins[2], J. Afonso[3], M. Sullivan[4], B. Mobasher[5],
L. E. Cram[6]

[1] *Imperial College of Science Technology and Medicine, Blackett Laboratory, Prince Consort Rd, SW7 2BZ, London, UK*
[2] *School of Physics, Bldg A29, University of Sydney, NSW 2006, Australia*
[3] *Centro de Astronomia da Universidade de Lisboa, Observatório Astronómico de Lisboa, 1349-018 Lisboa, Portugal*
[4] *Department of Astronomy and Astrophysics, University of Toronto, 60 St. George Street, Toronto, ON M5S 3H8, Canada*
[5] *Space Telescope Science Institute, 3700 San Martin Drive, Baltimore, MD 21218, USA*
[6] *The Australian National University, Canberra ACT 0200, Australia*

5 February 2008

ABSTRACT

We estimate the star-formation rates and the stellar masses of the Extremely Red Objects (EROs) detected in a $\approx 180\,\mathrm{arcmin}^2$ Ks-band survey ($Ks \approx 20\,\mathrm{mag}$). This sample is complemented by sensitive 1.4 GHz radio observations ($12\mu\mathrm{Jy}\ 1\sigma$ rms) and multiwaveband photometric data ($UBVRIJ$) as part of the Phoenix Deep Survey. For bright $K < 19.5\,\mathrm{mag}$ EROs in this sample ($I - K > 4\,\mathrm{mag}$; total of 177) we use photometric methods to discriminate dust-enshrouded active systems from early-type galaxies and to constrain their redshifts. Radio stacking is then employed to estimate mean radio flux densities of ≈ 8.6 (3σ) and $6.4\,\mu\mathrm{Jy}$ (2.4σ) for the dusty and early-type subsamples respectively. Assuming that dust enshrouded active EROs are powered by star-formation the above radio flux density at the median redshift of $z = 1$ translates to a radio luminosity of $L_{1.4} = 4.5 \times 10^{22}\mathrm{W/Hz}$ and a star-formation rate of $\mathrm{SFR} = 25\,\mathrm{M}_\odot\,\mathrm{yr}^{-1}$. Combining this result with photometric redshift estimates we find a lower limit to the star-formation rate density of $0.02 \pm 0.01\,\mathrm{M}_\odot\,\mathrm{yr}^{-1}\,\mathrm{Mpc}^{-3}$ for the $K < 19.5\,\mathrm{mag}$ dusty EROs in the range $z = 0.85 - 1.35$. Comparison with the star-formation rate density estimated for previous ERO samples (with similar selection criteria) using optical emission lines, suffering dust attenuation, suggests a mean dust reddening of at least $E(B - V) \approx 0.5$ for this population. We further use the Ks-band luminosity as proxy to stellar mass and argue that the dust enshrouded starburst EROs in our sample are massive systems, $\mathrm{M} \gtrsim 5 \times 10^{10}\,\mathrm{M}_\odot$. We also find that EROs represent a sizable fraction (about 50 per cent) of the number density of galaxies more massive than $\mathrm{M} = 5 \times 10^{10}\,\mathrm{M}_\odot$ at $z \approx 1$, with almost equal contributions from dusty and early type systems. Similarly, we find that EROs contribute about half of the mass density of the Universe at $z \approx 1$ (with almost equal contributions from dusty and early types), after taking into account incompleteness because of the magnitude limit $K = 19.5\,\mathrm{mag}$.

Key words: Surveys – cosmology: galaxies: mass function – galaxies: evolution – infrared: galaxies

1 INTRODUCTION

The class of Extremely Red Objects (EROs; $R - K > 5$, $I - K > 4\,\mathrm{mag}$), first identified more than 15 years ago (Elston et al. 1988), is believed to comprise a heterogeneous population of $z \gtrsim 1$ systems split between passive galaxies and dust enshrouded AGNs/starbursts (Cimatti et al. 2003). The identification of either type of galaxies (early or dusty) at high-z has important cosmological implications, thus providing significant impetus in ERO studies.

For example, finding early-type massive systems at high-z can provide information on both the galaxy forma-

⋆ email: a.georgakakis@imperial.ac.uk

tion redshift (Spinrad et al. 1997; Cimatti et al. 2002) and the global mass assembly (e.g. Fontana et al. 2003, 2004; Drory 2004; Glazebrook 2004), thus constraining galaxy formation scenarios: Monolithic collapse early in the Universe ($z_f > 2-3$) followed by passive evolution (e.g. Eggen et al. 1962; Larson 1975) versus hierarchical merging and relatively recent formation epochs (Baugh et al. 1996; Kauffmann 1996). Similarly a population of $z \gtrsim 1$ dusty active galaxies, AGNs or starbursts, that are missing from UV/optical surveys may play an important role in the global star-formation history (e.g. Haarsma et al. 2000; Smail et al. 2002; Hopkins 2004), the evolution of AGNs and the interpretation of the diffuse X-ray Background with respect to the (still) elusive population of high-z obscured QSOs (e.g. Hasinger et al. 2003).

Recent developments in instrumentation have yielded large ERO samples allowing systematic study of their statistical properties in a cosmological context. Cimatti et al. (2002) used optical spectroscopy from the K20 survey to explore the star-formation rates (SFR) of $K < 19.2$ mag EROs and to assess their contribution to the global star-formation history. Under conservative assumptions about reddening, these authors find that dust-enshrouded EROs represent a small but non-negligible fraction (about 10 per cent) of the SFR density at $z \approx 1$. Dust obscuration issues, however, make this result uncertain. Smail et al. (2002) expanded on the Cimatti et al. (2002) study using deep radio imaging to explore the SFR of $K < 20.5$ mag EROs independent of dust induced biases. Using this deeper K-band sample they estimate star-formation densities higher than those of Cimatti et al. (2002) and suggest that obscured galaxies make a sizable contribution to the total SFR density at $z \approx 1$. More recently Caputi et al. (2005) used the GOODS-South data to investigate the evolution of K-band selected galaxies. They argue that EROs among their sample constitute a sizable fraction (about 50-70 per cent) of galaxies with stellar mass $M > 5 \times 10^{10} \, M_\odot$ at $z = 1 - 2$, suggesting that they represent a major component of the stellar mass build-up at these redshifts.

The observational developments above are also complemented with efforts to model EROs using either semi-analytical (e.g. Somerville et al. 2004a) or hydrodynamical (e.g. Nagamine et al. 2005) methods. Despite significant progress, accounting for both the red colours and the number density of EROs remains a challenge for these numerical simulations. Part of the difficulty lies in our poor understanding of some of the properties of EROs. Open questions include what are the dust properties of these systems, what is the number density of dusty and early type EROs, what is the relative contribution of these sub-populations to the mass density.

In this paper we add to the discussion on the cosmological significance of EROs by combing an $\approx 180 \, \mathrm{arcmin}^2$ deep ($Ks \approx 20$ mag) Ks-band survey with ultra-deep 1.4 GHz radio data ($\approx 60 \, \mu$Jy) carried out as part of the Phoenix Deep Survey (Hopkins et al. 2003). This sample has already been used to explore the clustering properties and the environment of EROs (Georgakakis et al. 2005). The advantage of our survey is depth combined with wide area coverage reducing cosmic variance issues. Additionally, the ultra-deep radio data allow SFR estimates for EROs free from the dust obscuration effects that are expected to be impor-

tant in this class of sources. Throughout the paper we adopt $H_o = 70 \, \mathrm{km \, s^{-1} \, Mpc^{-1}}$, $\Omega_M = 0.3$ and $\Omega_\Lambda = 0.7$.

2   THE PHOENIX DEEP SURVEY

The Phoenix Deep Survey (PDS[†]) is an on-going survey studying the nature and the evolution of sub-mJy and μJy radio galaxies. Full details of the existing radio, optical and near-infrared (NIR) data can be found in Hopkins et al. (2003), Sullivan et al. (2004) and Georgakakis et al. (2005); here we summarise the salient details. The radio observations were carried out at the Australia Telescope Compact Array (ATCA) at 1.4 GHz during several campaigns between 1994 and 2001, covering a 4.56 square degree area centered at RA(J2000)=$01^h 11^m 13^s$ Dec.(J2000)=$-45°45'00''$. A detailed description of the radio observations, data reduction and source detection are discussed by Hopkins et al. (1998, 1999, 2003). The observational strategy adopted resulted in a radio image that is homogeneous within the central ≈ 1 deg radius, with the 1σ rms noise increasing from 12μJy in the most sensitive region to about 90μJy close to the edge of the $4.56 \, \mathrm{deg}^2$ field. The radio source catalogue consists of a total of 2148 radio sources to a limit of $60 \, \mu$Jy (Hopkins et al. 2003).

The Ks-band NIR data of the central region of the PDS were obtained using the SofI infrared instrument at the 3.6 m ESO New Technology Telescope (NTT). The observational strategy and details of the data reduction, calibration and source detection are described by Sullivan et al. (2004). The Ks-band mosaic covers a $13.5 \times 13.3 \, \mathrm{arcmin}^2$ area with a 45 min integration time, and a central $4.5 \times 4.5 \, \mathrm{arcmin}^2$ subregion which has an effective exposure time of 3 h. The completeness limit is estimated to be $Ks \approx 20$ mag for the full mosaic and $Ks \approx 20.5$ mag for the deeper central subregion.

Additional J-band NIR data of the central region of the PDS have been obtained using the InfraRed Imaging Spectrograph 2 (IRIS2) mounted at the f/8 focus of the 3.9 m Anglo-Australian telescope. These observations were carried out in 2003 September 8 in photometric conditions. The IRIS2 is equipped with a 1024x1024 HgCdTe array giving at the f/8 focus a pixel scale of 0.45 arcsec and a field of view of $7.7' \times 7.7'$. For the observational strategy a dithering pattern was adopted that consisted of a sequence of 60 s integrations followed by an offset of the telescope (maximum shift 75 arcsec). To get accurate sky frames the offset vector was not replicated between successive exposures. A single pointing was obtained with a total integration time of 1.8 hours.

The data reduction was carried out using IRAF tasks. The flat field frame was constructed using both the target observations and the dome flat following the method developed by Peter Witchalls and Will Saunders and described by Sullivan et al. (2004). The individual sky-subtracted images of the pointing were then combined to produce the final mosaic which has a useful area, after clipping noisy regions close to the field edge, of about $8 \times 8 \, \mathrm{arcmin}^2$. Photometric calibration was carried out using standard stars from Persson et al. (1998). The photometric solution has an rms

---

[†] http://www.atnf.csiro.au/people/ahopkins/phoenix/

scatter of about 0.02 mag. Astrometric calibration was performed using the positions of about 40 stars from the SUPERCOSMOS catalogue. This solution has an rms scatter of about 0.2 arcsec. The completeness limit is estimated to be $J \approx 21.5$ mag.

Deep multicolour imaging ($UBVRI$) of the PDF has been obtained using the Wide Field Imager at the AAT ($BVRI$-bands) and the Mosaic-II camera on the CTIO-4m telescope (U-band), fully overlapping the SofI Ks-band survey. Full details on the data reduction, calibration and source detection are again presented in Sullivan et al. (2004). In this study we will use the I-band observations, these being the deepest ($I \approx 24.2$ mag; see next section) and most appropriate for identifying EROs.

3 THE ERO SAMPLE AND PHOTOMETRIC REDSHIFTS

The ERO sample selection is described in detail by Georgakakis et al. (2005). In brief EROs are selected to have $I - K \geq 4$ mag. The 5σ detection threshold for the I-band catalogue is 24.2 mag, sufficiently deep to identify EROs with $Ks = 20$ mag. We find a total of 289 EROs to this magnitude limit within the 13.5×13.3 arcmin^2 area of our survey. To avoid incompleteness at faint Ks-band magnitudes and low signal-to-noise ratio data, in the analysis that follows we consider only those EROs with $K < 19.5$ mag, giving a total of 177 sources.

In the absence of optical spectroscopy we attempt to classify the ERO sample into different types, dusty and evolved, using their multiwaveband photometric properties. We adopt a method similar to that described by Smail et al. (2002) to fit two different template SED families ("dusty" or "old") to the optical/NIR magnitudes of EROs. We use the HYPER-Z code (Bolzonella, Miralles & Pelló 2000) to estimate photometric redshifts and to assess the goodness of fit for the two set of models. We then adopt the model and the corresponding photometric redshift that best fits the observations (minimum χ^2). In the case of dusty systems we adopt a continuous star-formation model with Salpeter IMF and solar metallicity as implemented in the new isochrone synthesis code of Bruzual & Charlot (2003). The reddening is allowed to vary in the range $A_V = 1 - 4$ (e.g. Cimatti et al. 2002) assuming the extinction curve of Calzetti et al. (2000). For evolved galaxies we use a model SED with exponentially declining star-formation rate with e-folding time of 1 Gyr, Salpeter IMF and solar metallicity (Bruzual & Charlot 2003). Only mild reddening is allowed for this set of template SEDs with $A_V < 0.5$. To minimise spurious redshift estimates we consider only those EROs with $K < 19.5$ mag and at least 3 band detections. The latter excludes from the sample a total of 40 sources, i.e. about 20 per cent of the $K < 19.5$ mag sample. Each ERO is assigned the template (dusty or old) and the corresponding photometric redshift that gives the minimum χ^2. For a small number of sources (14) neither dusty nor old SEDs can provide an acceptable fit, both giving $\chi^2 > 2.7$, i.e. rejection of the model templates at the > 90 per cent confidence level. These 14 systems are excluded from the analysis. We note that these sources either have more complex SEDs that those assumed here, are associated with QSO dominated sources or are Galactic stars,

e.g. late type cool dwarfs (e.g. Francis et al. 2004). For example 4 of the 14 sources are assigned SEXTRACTOR flag CLASS_STAR$= 0.93 - 0.95$ only marginally lower than the cutoff used for star/galaxy separation (CLASS_STAR> 0.95; Georgakakis et al. 2005). The final sample comprises a total of 123 $K < 19.5$ mag EROs.

The method above clearly, cannot reproduce complex SEDs with contributions from both evolved and young obscured stellar populations. Nevertheless, it provides a rough classification allowing an assessment of the relative fraction of EROs at the two extremes: Old and passively evolving vs young, reddened systems. Some fraction of misclassifications are however, inevitable in the scheme above that relies on broad-band optical/NIR photometry to differentiate between dusty and old EROs. Moreover, some of the EROs in the sample do not have J-band photometry available, which is sensitive to the H+K spectral break of evolved galaxies at $z \gtrsim 1$. This is likely to introduce further uncertainty into the classification. Also, a fraction of EROs are expected to harbor type-II AGN activity. Here we assume that it is the host galaxy stellar population, rather than the obscured AGN that dominates the broad-band optical/NIR colours of these systems. Observations of X-ray selected obscured AGNs both at moderate and higher-z suggest that their continuum emission is indeed dominated by the host galaxy rather than the central engine (e.g. Gandhi et al. 2004; Georgakakis et al. 2004; Mobasher et al. 2004).

Figure 1 presents the $I - K$ against $J - K$ colour-colour plot introduced by Mannucci & Pozzetti (2001) to discriminate between dusty active and evolved EROs. Only sources in our sample with available J-band photometry (detection or upper limit) are plotted here. There is reasonable agreement between the classification using the SED template fitting method and the optical/NIR colours of our sample. Figure 2 plots the redshift distribution of the $K < 19.5$ mag EROs that are best-fit by early-type and dusty templates separately. These are broadly consistent with the distributions discussed by Daddi et al. (2001) and Roche et al. (2003). Also shown in Figure 2 are the spectroscopic redshift distribution of $K < 19.2$ mag EROs from the K20 survey (Cimatti et al. 2002). There is reasonable agreement with our photometric redshift estimates, although we find more $z \gtrsim 1.3$ early type EROs. At these redshifts however, Cimatti et al. (2002) discuss that instrumental issues are likely to affect the identification of absorption-line systems resulting in incompleteness.

To compare the properties of $K < 19.5$ mag EROs with those of the full K-band selected population, we also apply the above photometric redshift estimation method to all $K < 19.5$ mag non-ERO galaxies (i.e. $I - K < 4$ mag; total of 1208). Spectroscopic redshift information available for the brighter of these systems (total of 28) is used to assess the accuracy of the results. The 1 sigma rms uncertainty of the quantity $\delta z = z_{phot} - z_{spec}$ is estimated 0.06.

4 RADIO DETECTED EROS

A total of 95 radio sources brighter than 60μJy overlap with the Ks-band survey region. Using a matching radius of 2 arcsec we find that 17 of them are associated with EROs, 14 of which have $K < 19.5$ mag. The fraction of $K < 19.5$ mag
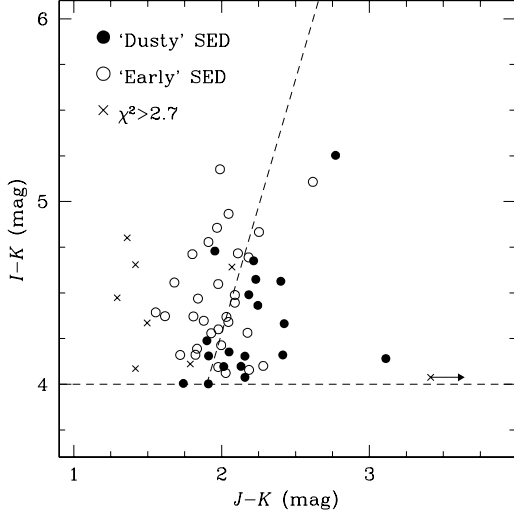
Figure 1. $I - K$ against $J - K$ colour plot. The horizontal line shows our ERO selection $I - K > 4$ mag. The diagonal dotted line, introduced by Mannucci & Pozzetti (2001), discriminates between early (on the left) and dusty (to the right) systems. The filled and open circles are $K < 19.5$ mag EROs in the PDS that are best fit by dusty and early template SEDs respectively. Crosses correspond to EROs for which the template fitting method described in the text does not provide an acceptable fit to the observations, giving $\chi^2 > 2.7$.

EROs with radio counterparts is 8 ± 2 per cent (14/177). This is a factor of 2 higher than the fraction of non-EROs ($I - K < 4$ mag) at the same magnitude limit with radio counterparts (4 ± 1 per cent), suggesting a higher fraction of dusty active systems among the ERO population. The properties of the radio matched EROs are presented in Table 1. About half of the radio emitting EROs are best-fit by dusty SEDs (8/17) with the remaining half assigned either early type templates (4/17) or no SED (5/17). Three of the dusty sources are assigned redshifts $z < 0.8$ lower than that expected for EROs (i.e. $z \approx 1$). These are interesting objects in their own right, since the k-correction does not strongly contribute to the red colors observed. They may resemble the ERO already studied in the PDS, PDFJ011423 (Afonso et al. 2001), an extreme example of a dusty star-forming dominated ERO at relatively low redshift, $z = 0.65$.

Assuming that the radio emission is due to starburst activity and adopting the relation between radio luminosity ($L_{1.4\,GHz}$) and star-formation rate (SFR) of Bell et al. (2003) we estimate SFRs for stars in the mass range $0.1 - 100\,M_\odot$ of about $10^2 - 10^3\,M_\odot\,yr^{-1}$ for EROs at $z \approx 1$. Also, adopting the radio-FIR correlation (Helou, Soifer & Rowan-Robinson 1985) we estimate FIR luminosities of about $10^{11} - 10^{12}\,L_\odot$ placing these systems in the class of Luminous and Ultra-Luminous Infrared Galaxies (LIGs; ULIGs).

5   RADIO STACKING

For EROs that are not detected in the PDS radio survey we provide an estimate of their mean radio properties using the stacking analysis method described by Hopkins et
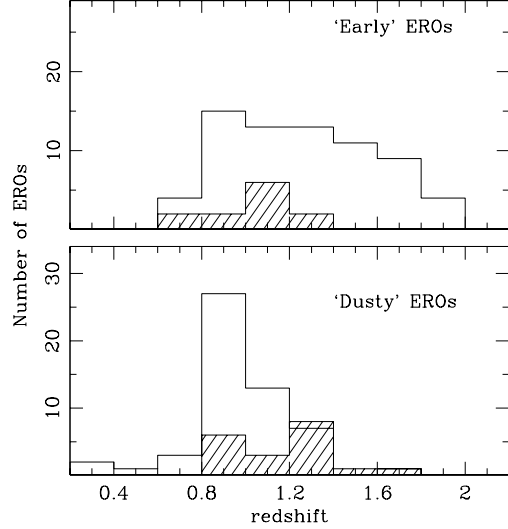
Figure 2. Open histograms are the photometric redshift distribution of the $K < 19.5$ mag EROs in the PDS that are best fit with early (upper panel) or dusty (lower panel) template SEDs. For comparison we also plot the spectroscopic redshift distribution of $K < 19.2$ mag EROs identified in the K20 survey.

al. (2004) and Georgakakis et al. (2005). We extract sub-images from the radio mosaic at the location of the non-radio detected EROs, and construct the weighted average of the sub-images (weighted by $1/rms^2$, to maximise the resulting signal-to-noise, since the radio mosaic has a varying noise level over the image). Sub-images where low S/N emission ($> 1.5\,\sigma$) is present at the location of the non-detected source are excluded from the stacking, in order to avoid biasing the stacking signal result by the presence of a small number of low S/N sources. The stacking analysis above is applied separately to systems that are best-fit by the dusty and early-type templates. The results are presented in Table 2. For the dusty EROs we estimate a mean radio flux density of $8.6\,\mu Jy$ significant at the 3σ confidence level (1σ rms of $2.8\,\mu Jy$). This signal is likely to be associated with obscured star-formation activity in the host galaxy, the stacked image has an rms noise of $2.7\,\mu Jy$, and a marginally significant, 2.4σ, detection at $6.4\,\mu Jy$. The radio emission in these evolved systems may arise in low-level AGN activity.

To test the sensitivity of these results to the dusty/early type classification scheme based on SED template fitting, we also use the Pozzetti & Mannucci (2001) $I - K$ vs $J - K$ plot to segregate EROs into different types and repeat the stacking analysis. Only the smaller subsample of EROs with J-band information available are used. The results are also given in Table 2. We estimate mean flux densities of 6.0 and $7.5\,\mu Jy$ for dusty and early EROs respectively, albeit with lower statistical significance, 1.6 and 2.3σ respectively, because of the smaller number of sources involved in the stacking. Nevertheless, these estimates are in reasonable agreement, within the uncertainties, with those found using the classification based on template fitting, suggesting our results are robust.

At the mean redshift of dusty and early type EROs estimated in section 3 the mean flux densities above (using the

#	$\alpha_{1.4}$ (J2000)	$\delta_{1.4}$ (J2000)	δr (arcsec)	I (mag)	J (mag)	K (mag)	$S_{1.4}$ (mJy)	z	χ^2	$P_{1.4}$ (W/Hz)	SFR ($M_\odot$/yr)
1	01 10 54.10	$-45\ 50\ 02.54$	0.8	23.41 ± 0.04	–	18.94 ± 0.04	0.070	$1.40^{+0.04}_{-0.04}$	1.19	24.00	–
2	01 10 58.82	$-45\ 51\ 29.48$	0.6	22.77 ± 0.02	–	18.22 ± 0.03	0.100	$0.92^{+0.09}_{-0.06}$	0.31	23.69	276
$3^\star$	01 11 00.91	$-45\ 49\ 39.67$	1.6	>24.50	–	19.77 ± 0.06	0.109	–	–	–	–
4	01 11 02.63	$-45\ 51\ 34.96$	0.1	21.67 ± 0.01	–	17.59 ± 0.02	0.222	$0.54^{+0.02}_{-0.04}$	1.00	23.45	158
5	01 11 03.81	$-45\ 51\ 18.10$	0.7	21.96 ± 0.01	–	17.48 ± 0.02	0.086	$0.62^{+0.14}_{-0.06}$	0.25	23.19	86
6	01 11 09.66	$-45\ 48\ 19.43$	1.1	23.47 ± 0.03	21.01 ± 0.17	19.13 ± 0.04	0.084	$1.22^{+0.05}_{-0.01}$	0.65	23.93	–
7	01 11 13.13	$-45\ 51\ 23.11$	0.8	23.32 ± 0.03	–	18.83 ± 0.04	0.077	$1.35^{+0.06}_{-0.04}$	0.35	24.01	–
8	01 11 14.21	$-45\ 50\ 03.21$	0.7	22.36 ± 0.02	–	18.01 ± 0.02	0.152	–	> 2.7	–	–
9	01 11 14.20	$-45\ 42\ 49.94$	0.9	22.21 ± 0.02	19.88 ± 0.07	17.98 ± 0.02	0.086	$0.25^{+0.05}_{-0.01}$	1.15	22.27	10
10	01 11 15.23	$-45\ 41\ 00.51$	0.3	22.92 ± 0.02	–	18.28 ± 0.03	0.138	$1.19^{+0.08}_{-0.01}$	2.61	24.12	735
11	01 11 25.33	$-45\ 47\ 24.74$	1.0	23.10 ± 0.02	21.35 ± 0.21	18.94 ± 0.04	0.148	$0.98^{+0.10}_{-0.24}$	0.24	23.93	480
12	01 11 36.53	$-45\ 41\ 54.74$	1.2	22.12 ± 0.01	>21.50	18.08 ± 0.03	0.101	–	> 2.7	–	–
13	01 11 37.00	$-45\ 40\ 36.98$	1.9	23.05 ± 0.02	–	18.99 ± 0.04	0.246	$0.90^{+0.08}_{-0.09}$	0.33	24.06	641
$14^\star$	01 11 58.39	$-45\ 40\ 28.28$	1.6	>24.50	–	19.70 ± 0.07	0.089	–	–	–	–
15	01 12 00.65	$-45\ 39\ 41.33$	0.6	22.94 ± 0.02	–	18.70 ± 0.04	0.138	$0.82^{+0.05}_{-0.03}$	2.05	23.71	–
16	01 12 07.51	$-45\ 46\ 16.28$	0.5	23.70 ± 0.04	–	18.40 ± 0.02	0.101	$1.13^{+0.05}_{-0.02}$	0.96	23.93	470
$17^\star$	01 12 05.82	$-45\ 46\ 02.30$	0.5	24.09 ± 0.04	–	19.64 ± 0.04	0.070	–	–	–	–

*No photometric redshift estimated because detected in less than 3 filters.

The columns are: 1: ID number; 2, 3: right ascension and declination in J2000 of radio centroid; 4: radio/K-band position offset; 5, 6, 7: I, J, K-band magnitudes; 8: radio flux density; 9, 10: photometric redshift and χ^2 of the best fit. When $\chi^2 > 2.7$ no photo-z is listed; 11: radio power; 12: SFR for those sources only that are best-fit by dusty SEDs.

Table 1. The properties of EROs with radio counterparts.

SED fitting classification) translate to 1.4 GHz luminosities of 4.5×10^{22} and $3.4 \times 10^{22}\ \mathrm{W\,Hz^{-1}}$ respectively. We use a k-correction assuming a power law spectral energy distribution of the form $S_\nu \propto \nu^{-\alpha}$ with $\alpha = 0.8$. In the case of evolved EROs, the observed mean radio luminosity may originate in low-level AGN activity, found in many ellipticals. Indeed, the stacking analysis provides sensitivities well below the radio-loud AGN limit ($\approx 10^{24}\mathrm{W/Hz}$; Ledlow & Owen 1996), allowing the detection of signal from lower luminosity systems. For the the dusty subsample the observed mean radio emission is likely associated with starburst activity (e.g. LIGs; Sadler et al. 2002). Assuming this is the case, the mean radio luminosity of the dusty sub-population corresponds to an average $\mathrm{SFR}(0.1-100\,M_\odot) \approx 25\,M_\odot\ \mathrm{yr^{-1}}$, adopting the calibration of Bell (2003). This is of the same order of magnitude as the mean ERO SFR estimate of Yan et al. (2004), $\approx 50\,M_\odot\ \mathrm{yr^{-1}}$, based on $24\mu m$ Spitzer observations of the ELAIS-N1 region. The factor of two difference can be explained by the fact that Yan et al. (2004) take the mean of the $24\mu m$ flux distribution of EROs detected at these wavelength and convert that to SFR assuming $z = 1$. If we instead take the mode of their distribution, which is more representative of the full dusty ERO population and comparable to the statistical analysis presented here, we find excellent agreement with our results.

6 STAR FORMATION RATE DENSITY

In this section we use the radio emission of $Ks < 19.5$ mag dusty EROs to explore their contribution to the global SFR density at $z \approx 1$. For those EROs that do not have a detected radio counterpart we use the stacking analysis results of section 5. We further assume that the radio flux density of the

sample	number of sources	$S_{1.4}$ (μJy)	significance
SED fitting classification			
dusty	48	8.6	3.0σ
early	47	6.4	2.6σ
$I - K$ vs $J - K$ classification			
dusty	23	6.0	1.6σ
early	26	7.5	2.3σ

Table 2. Radio stacking results.

dusty ERO sub-population is dominated by star-formation rather than AGN emission. This is a reasonable assumption since X-ray surveys suggest that only 3-14 per cent of EROs have X-ray counterparts likely to be associated with obscured AGN (Brusa et al. 2005 and references therein). The upper limit in the X-ray/ERO identification rate range above occurs in the ultra-deep Chandra surveys (Alexander et al. 2003) that are sufficiently sensitive to detect X-ray emission from powerful starbursts at $z \approx 1$. A fraction of the X-ray/ERO associations in these fields are therefore, dominated by star-formation rather than AGN activity. Moreover, only a small fraction of the AGN population (≈ 10 per cent) show radio emission while, the radio properties of some obscured AGNs are suggested to be dominated by powerful starburst activity (e.g. Bauer 2002; Georgakakis et al. 2004). The evidence above suggests that contamination of our sample by AGN is likely to have little impact on the ERO star-formation density estimation.

We first determine the radio luminosity density using the photometric redshift information to estimate the effective cosmological volume probed by the Ks-selected sample (e.g. $Ks < 19.5$ mag) using the standard $1/V_{max}$ formalism (e.g. Lilly et al. 1996; Mobasher et al. 1999). The radio luminosity density is then converted to SFR density using the calibration of Bell [2003; SFR(M $= 0.1 - 100$ M$_\odot$) $=$ L$_{1.4}/1.81 \times 10^{21}$, for $L_{1.4} > 6.4 \times 10^{21}$ W Hz^{-1}]. For this exercise we only consider EROs that are best-fit by dusty template SEDs and have photometric redshifts in the range $z = 0.85 - 1.35$ (total of 41). We estimate a radio luminosity density of $(3.6 \pm 1.8) \times 10^{19}$ W Hz^{-1} Mpc^{-3} corresponding to $\rho_\star$(M $= 0.1 - 100$ M$_\odot$) $= 0.02 \pm 0.01$M$_\odot$ yr^{-1} Mpc^{-3}. The dominant source of uncertainty in this estimate is cosmic variance, which is assumed to be about 50 per cent of the ERO number counts (Somerville et al. 2004b). As discussed in section 3 about 30 per cent of the $K < 19.5$ mag EROs are excluded from the analysis because the either have poor data (detected in less than 3 bands) or are not well fit ($\chi^2 > 2.7$) by the template SEDs used in this study. Assuming that this population has similar redshift distribution and classification mix (e.g. dusty vs early) with the $K < 19.5$ mag EROs used in our analysis, the SFR density above should be revised upward by about 30 per cent. In the analysis that follows we do not take into account this moderate incompleteness correction.

Our results are plotted in Figure 3 at the median redshift of ≈ 1 in comparison with the compilation of SFR densities from different wavelengths of Hopkins (2004). The $K < 19.5$ mag dusty ERO estimate accounts for about 10 per cent of the total SFR density estimated at $z \approx 1$ (≈ 0.15M$_\odot$ yr^{-1} Mpc^{-3}). The fraction above should be considered a lower limit however, since it does not take into account EROs fainter than $Ks = 19.5$ mag. This suggests that dust enshrouded starburst activity in EROs is potentially a non-negligible component of the global SFR at these redshifts.

Cimatti et al. (2002) used the K20 sample with a magnitude cutoff $K < 19.2$ mag, similar to the present study, and found $\rho_\star \approx 0.015$ M$_\odot$ yr^{-1} Mpc^{-3} in the range $z = 0.85 - 1.3$, in fair agreement with our result. Unlike our study however, these authors used the [OII] 3727Å line as a SFR estimator and applied a mean dust correction of $E(B - V) \approx 0.5$, which was found to be consistent with the average UV/optical continuum of emission-line EROs in their sample. The agreement between our dust-independent estimate and that of Cimatti et al. (2002), after taking into account reddening, suggests that a mean dust extinction of at least $E(B - V) \approx 0.5$ is required to provide an unbiased view of the ERO star-forming population. It is interesting to note that recent hydrodynamical simulations by Nagamine et al. (2005) also invoke a uniform extinction of $E(B - V) \approx 0.4$ for their model galaxies to explain the red observed colours of EROs.

Smail et al. (2002) used deep radio data (1.4 GHz) to estimate the SFR density of $K < 20.5$ mag EROs in the range $z = 0.8 - 1.5$. We consider their dusty ERO subsample (total of 20) classified on the basis of SED template fitting. This is directly comparable to the ERO sample used here to estimate the SFR density. Using the $L_{1.4}$-to-SFR conversion adopted here, we estimate a SFR density of $\rho_\star$(M $= 0.1 - 100$ M$_\odot$) ≈ 0.04 M$_\odot$ yr^{-1} Mpc^{-3} for the

Smail et al. (2002) $K \approx 20.5$ mag dusty EROs. This factor of 2 difference compared to our estimate suggests that EROs fainter than our $K = 19.5$ mag limit make a large contribution to the SFR density at $z \approx 1$, and the ERO component may in fact be a large contribution (about 25 per cent) to the SFR density at this redshift. Indeed, Smail et al. argue that the observed break in the number counts of EROs at $K \approx 19.5$ (McCarthy et al. 2001; Smith et al. 2002) is because passive EROs make a sizable contribution to the counts at bright magnitudes ($K \lesssim 20$ mag) while dusty active EROs make up the bulk of the population at fainter limits. We also note that incompleteness corrections in the Smail et al. (2002) SFR density (e.g. sources that are not well fit by their template SEDs) would revise their result upward by about 45 per cent increasing it to $\rho_\star$(M $= 0.1 - 100$ M$_\odot$) ≈ 0.06 M$_\odot$ yr^{-1} Mpc^{-3} (using the $L_{1.4}$-to-SFR conversion adopted here). This incompleteness correction is comparable to that estimated for the PDS EROs.

In the next section we will present evidence that the $K < 19.5$ ERO sample and the dusty sub-population in particular, are likely to be complete to the stellar mass limit M $\approx 5 \times 10^{10}$ M$_\odot$. This combined with the above results suggests that about half of the dusty ERO SFR density at $z \approx 1$ arises in systems with mass $\gtrsim 5 \times 10^{10}$ M$_\odot$ (i.e. those detected in this study) with the remaining half in less massive galaxies fainter than $K \approx 19.5$ mag. This is in contrast to the local Universe where the most massive galaxies have little, if any, on-going star-formation activity (e.g. Kauffmann et al. 2004). This trend continues to $z \approx 1$ although at these redshifts numerous studies also find evidence for a population of massive galaxies that experience starburst activity in agreement with our result (e.g. Cowie et al. 1996; Drory et al. 2004; Fontana et al. 2004).

7 STELLAR MASS DENSITY

Next we estimate the stellar mass density of EROs at $z \approx 1$ in comparison with that of the full sample of K-band selected galaxies with $K < 19.5$. Galaxy masses are estimated using K-band luminosities and the mass–to–light ratio, M/L_K, of the best fit SED for each system (e.g. Caputi et al. 2005). These are in fair agreement with the mean M/L_K ratios of NIR selected galaxies at $z = 1.0 - 1.5$ estimated by Fontana et al. (2004) from the K20 sample (http://www.arcetri.astro.it/~k20). These authors estimate stellar masses by fitting a range of template SEDs to multi-waveband photometry ($UBVRIzJKs$) of spectroscopically identified $K < 20$ mag galaxies. They adopt a grid of SEDs with exponentially declining star-formation rates, a Salpeter IMF and an SMC extinction law to estimate M/L_K ratios in the redshift range $0 \lesssim z \lesssim 2$.

The estimated masses, particularly for early-type EROs, are likely to be representative of the population. This is because compared to shorted wavelengths the K-band is more closely associated to the integrated galaxy stellar mass, is less affected by bursts of star-formation, dust extinction, and the galaxy type, while there is only weak dependence of the M/L_K on redshift. We caution the reader however, that dusty EROs are more difficult to model and to estimate mean M/L_K ratios for, since they are likely to have
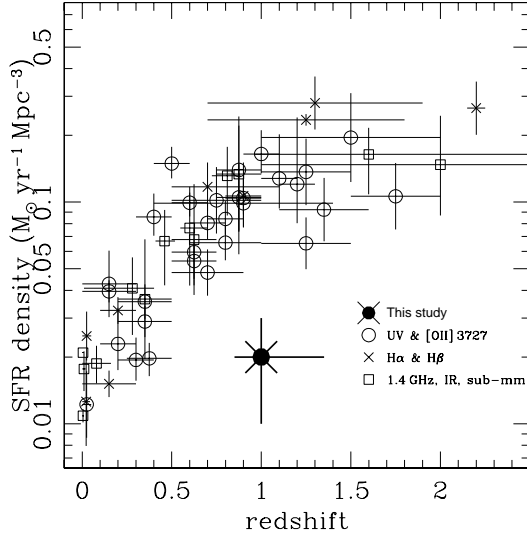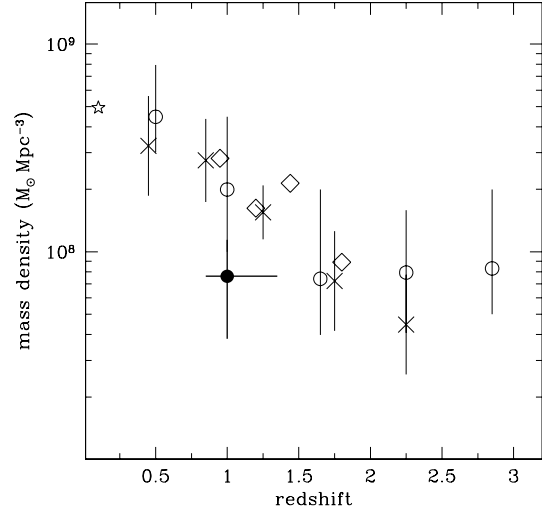
Figure 3. Global SFR density density as a function of redshift. The filled crossed circle is the $K < 19.5$ mag EROs contribution estimated in this paper plotted at the median redshift of the sample, $z = 1$. This is compared with global SFR density compilation of Hopkins (2004). Points are coded by rest frame wavelength used to estimate the SFR: open circles: UV; crosses: Hα and Hβ; 1.4 GHz, IR or sub-mm: open squares.

Figure 4. Global mass density as a function of redshift. The filled circle is the $K < 19.5$ mag ERO contribution estimated in this paper plotted at the median redshift of the sample, $z = 1$. Star: Cole et al. (2000); crosses: Fontana et al. (2004); open circles: Fontana et al. (2003); diamonds: Glazebrook et al. (2004).

mixed stellar populations, large extinction and complex dust covering factors.

We first estimate the number density of EROs in comparison with those of the full $K < 19.5$ mag sample using the standard $1/V_{max}$ method. We note that the magnitude limit $K = 19.5$ corresponds to a mass of $M \gtrsim 5 \times 10^{10}\,M_{\odot}$ at $z = 1$, adopting the mean k-corrections and mass-to-light ratios used here ($M/L_K \approx 0.6$). Our sample is therefore, nearly complete for galaxies more massive than $\gtrsim 5 \times 10^{10}\,M_{\odot}$. For the redshift range $0.85 - 1.35$ and $M > 5 \times 10^{10}\,M_{\odot}$ we estimate number densities of $(4.7 \pm 2.4) \times 10^{-4}\,\mathrm{Mpc}^{-3}$ for EROs and $(10.9 \pm 3.1) \times 10^{-4}\,\mathrm{Mpc}^{-3}$ for the full $K < 19.5$ mag galaxy population. The dominant source of uncertainty in these estimates is cosmic variance, which is assumed to be of about 50 and 30 per cent of EROs and non-EROs respectively (Somerville et al. 2004b). These densities are in good agreement with the results of Caputi et al. (2005) at similar redshifts. As also noted by these authors, EROs are a sizable component of galaxies more massive than $M > 5 \times 10^{10}\,M_{\odot}$ at $z \approx 1$, representing about 50 per cent of the population in the PDS. Moreover, both dusty and early-type EROs contribute almost equally to this fraction with number densities of about 2.7×10^{-4} and $2 \times 10^{-4}\,\mathrm{Mpc}^{-3}$. This suggests that both the dusty active and the early-type EROs at $z \approx 1$ have already assembled a sizable fraction of their stellar mass.

The evolution of EROs to $z = 0$ remains uncertain although elliptical galaxies are proposed as their descendants. Under this assumption we explore connections between the NIR properties of the two populations. The median luminosity of the PDS EROs is estimated $M_K = -25.1$ mag. Assuming passive evolution from $z = 1$ to the present day this luminosity corresponds to $M_K \approx -24.4$ mag at $z = 0$, i.e. similar to the characteristic absolute magnitude of local

ellipticals $M_K^* \approx -24.2$ mag (Kochanek et al. 2001). The evidence above suggests that if EROs evolve into nearby ellipticals they occupy the bright end ($L \gtrsim L^*$) of the luminosity function of these systems.

The mass density of early and dusty EROs at $z = 0.85 - 1.35$ are presented in Table 3 and are plotted in Figure 4. The errorbars are estimated assuming 50 per cent cosmic variance to the ERO number counts. Dusty and early type systems contribute almost equally to the ERO mass assembly at this redshift range. Figure 4 compares our results with estimates of the global mass density out to $z \approx 3$. Although there is some uncertainty in the determination of the total stellar mass density at $z \approx 1$, adopting a value of $\approx 2.5 \times 10^8\,M_{\odot}\,\mathrm{Mpc}^3$ we find that the $K < 19.5$ EROs represent about 30 per cent of that, suggesting that they are a non-negligible component of the mass assembly at this redshift. This fraction is likely to represent a lower limit since EROs fainter than the $Ks = 19.5$ are not taken into account. We address this point by comparing with the stellar mass density of all $K < 19.5$ mag galaxies in the range $0.85 < z < 1.35$. Any incompleteness biases are likely to affect both this and the EROs samples in almost the same way. We estimate a stellar mass density of $\rho_m = (1.7 \pm 0.5) \times 10^8\,M_{\odot}\,\mathrm{Mpc}^{-3}$ for $K < 19.5$ mag galaxies. Therefore the EROs studied here represent about 50 per cent of the stellar mass density of the full $Ks < 19.5$ sample. Although not *all* massive galaxies at $z \approx 1$ are EROs the evidence above underlines the significance of this population with regards to the mass assembly of the Universe at $z \approx 1$.

8   SUMMARY & CONCLUSIONS

In this paper we use an $\approx 180\,\mathrm{arcmin}^2$ Ks-band survey overlapping with ultra-deep radio observations and multiwave-

sample	number of sources	$\rho_m(> 5 \times 10^{10}\,M_\odot)$ $(M_\odot\,\mathrm{Mpc}^{-3})$	$\rho_\star(0.1 - 100\,M_\odot)$ $(M_\odot\,\mathrm{yr}^{-1}\,\mathrm{Mpc}^{-3})$
dusty	41	$4.1 \pm 2.0 \times 10^7$	0.02 ± 0.01
early	34	$3.5 \pm 1.7 \times 10^7$	–
all	75	$7.6 \pm 3.2 \times 10^7$	–

Table 3. Mass and SFR density for $K < 19.5$ EROs in the redshift range $0.85 < z < 1.35$.

band photometry ($UBVRIJ$) to estimate the SFRs and the stellar masses of EROs with $K < 19.5$ mag. Template SEDs are fit to the broad-band optical/NIR photometric data to discriminate between dusty and early-type EROs and to determine their photometric redshifts. This classification is found to be in fair agreement with methods using optical/NIR colours (e.g. $I - K$ vs $J - K$).

About 8 per cent of the $K \lesssim 19.5$ mag EROs have radio counterparts to the flux density limit of about $60\,\mu\mathrm{Jy}$. For the remaining sources we use radio stacking analysis to constrain their mean radio properties. We estimate a stacked signal of about 9 (3σ) and $6\,\mu\mathrm{Jy}$ (2.5σ) for dusty and early-type EROs respectively. Assuming that the radio emission in the dusty sub-population is due to star-formation activity we estimate a mean star-formation rate of $\mathrm{SFR} = 25\,M_\odot\,\mathrm{yr}^{-1}$ at $z = 1$ free from dust obscuration effects. The radio detected EROs at $z \approx 1$ have, on average, much higher SFRs in the range $100 - 1000\,M_\odot\,\mathrm{yr}^{-1}$. Combining these results with the photometric redshift estimates we find that the SFR density of the Universe in the range $0.85 - 1.35$ due to $K < 19.5$ mag EROs is $0.02 \pm 0.01\,M_\odot\,\mathrm{yr}^{-1}\,\mathrm{Mpc}^{-3}$. This should be considered a lower limit since EROs fainter than $K = 19.5$ mag are not taken into account. Comparison with deeper samples suggests that correcting for these biases will likely increase the estimate above by at least a factor of 2. We also argue that the systems responsible for the observed star-formation density are dusty starbursts more massive than $M = 5 \times 10^{10}\,M_\odot$. Less massive dusty EROs lie below the magnitude limit $K = 19.5$ mag at $z \approx 1$ and are the systems responsible for the missing (at least factor of 2) SFR density at $z \approx 1$. Comparison of the dust-independent SFR density estimated here with that of similarly selected ERO samples using optical emission lines, suffering dust attenuation, suggests a mean dust reddening of at least $E(B - V) \approx 0.5$ for this population.

We further use mass-to-light ratios of the best-fit template SED to convert the Ks-band luminosity of EROs to stellar mass. We find that EROs contribute about 50 per cent to the total number density of galaxies with stellar mass $M > 5 \times 10^{10}\,M_\odot$ at $z \approx 1$. This fraction is almost equally split between dusty and early type systems. We further estimate that the $K < 19.5$ EROs represent about 50 per cent of the global mass density in the redshift range $z = 0.85 - 1.35$, after taking into account incompleteness due to the magnitude limit $K = 19.5$ mag. This indicates that these systems are also a non-negligible component of the Universe mass build-up at these redshifts. The ERO mass density above is also almost equally split between the dusty and early type subpopulations.

REFERENCES

Afonso J., Mobasher B., Chan B., Cram L., 2001, ApJ, 559L, 101
Alexander D. M., et al., 2003, AJ, 126, 539
Bauer F. E., et al., 2002, AJ, 124, 2351
Bell E. F., 2003, ApJ, 586, 794
Bolzonella M., Miralles J.-M., Pelló R., 2000, A&A 363, 476
Brusa M., et al., 2005, A&A, 432, 69
Bruzual A. G., Charlot S., 2003, MNRAS, 344, 1000
Calzetti D., Armus L., Bohlin R. C., Kinney A. L., Koornneef J., Storchi-Bergmann T., 2000, ApJ, 533, 682
Caputi K. I., Dunlop J. S., McLure R. J., Roche N. D., 2005, MNRAS in press, astro-ph/0408373
Cimatti A., et al., 2003, A&A, 412L, 1
Cimatti A., et al., 2002, A&A, 381L..68
Cole S., Lacey C. G., Baugh C. M., Frenk C. S., 2000, MNRAS, 319, 168
Cowie L. L., Songaila A., Hu E. M., Cohen J. G., 1996, AJ, 112, 839
Daddi E., Broadhurst T., Zamorani G., Cimatti A., Rottgering H., Renzini A., 2001, A&A, 376, 825
Drory N., Bender R., Feulner G., Hopp U., Maraston, C., Snigula J., Hill G. J., 2004, ApJ, 608, 742
Eggen O. J., Lynden-Bell D., Sandage A. R., 1962, ApJ, 136, 748
Elston R., Rieke G. H., Rieke M. J., 1988, ApJ, 331L, 77
Fontana A., et al., 2003, ApJ, 594L, 9
Fontana A., et al., 2004, A&A, 424, 23
Francis P. J., Nelson B. O., Cutri R. M., 2004, AJ, 127, 646
Gandhi P., Crawford C. S., Fabian A. C., Johnstone R. M., 2004, MNRAS, 348, 529
Georgakakis A., Afonso J., Hopkins A. M., Sullivan M., Mobasher B., Cram L. E., 2005, ApJ, 620, 584
Georgakakis A., Hopkins A. M., Sullivan M., Afonso J., Mobasher B., Cram L. E., 2004, MNRAS, 354, 127
Georgakakis A, Mobasher B, Cram L., Hopkins A., Lidman C., Rowan-Robinson M., 1999, MNRAS, 306, 708.
Glazebrook K., et al., 2004, Nature, 430, 181
G. Hasinger G., 2003, Proceedings of the conference: "The restless high energy universe", Amsterdam, to be published in Nucl. Physics B. Suppl. Ser., editors E.P.J. van den Heuvel, J.J.M. in 't Zand, and R.A.M.J. Wijers, astro-ph/0310804
Helou G., Soifer B. T., Rowan-Robinson M., 1985, ApJ, 298L, 7
Hopkins A. M., 2004, ApJ, 615, 209
Hopkins A. M., Afonso J., Georgakakis A., Sullivan M., Mobasher B., Cram L. E., 2004, in "Multiwavelength Cosmology" conference, ed. M. Plionis, pg. 125, astro-ph/0309147
Hopkins A. M., Afonso J., Chan B., Cram L. E., Georgakakis A., Mobasher B., 2003, AJ, 125, 465
Hopkins A., Afonso J., Cram L., Mobasher B., 1999, ApJ, 519L, 59
Hopkins A. M., Mobasher B., Cram L., Rowan-Robinson M., 1998, MNRAS, 296, 839H

Kauffmann G., White S. D. M., Heckman T. M., Menard B., Brinchmann J., Charlot S., Tremonti C., Brinkmann J., 2004, MNRAS, 353, 713

Kauffmann G., 1996, MNRAS, 281, 487

Kochanek C. S., et al., 2001, 560, 566

Larson R. B., 1975, MNRAS, 173, 671

Ledlow M. J. & Owen F. N., 1996, AJ, 112, 9

Lilly S. J., Le Fevre O., Hammer F., Crampton D., 1996, ApJ, 460, L1

McCarthy P. J., et al., 2001, ApJ, 560, L31

Mobasher B., et al., 2004, ApJ, 600L, 167

Mobasher B., Cram L., Georgakakis A., Hopkins A., 1999, MNRAS, 308, 45

Nagamine K., Cen R., Hernquist L., Ostriker J. P., Springel V., 2005, ApJ, submitted, astro-ph/0502001

Persson S. E., Murphy D. C., Krzeminski W., Roth M., ieke M. J., 1998, AJ, 116, 2475

Pozzetti L., Mannucci F., 2000, MNRAS, 317L, 17

Roche N. D., Dunlop J., Almaini O., 2003, MNRAS, 346, 803

Sadler E., et al., 2002, MNRAS, 329, 227

Smail I., Owen F. N., Morrison G. E., Keel W. C., Ivison R. J., Ledlow M. J., 2002, ApJ, 581, 844

Smith G. P., et al., 2002, MNRAS, 330, 1

Spinrad H., Dey A., Stern D., Dunlop J., Peacock J., Jimenez R., Windhorst R., 1997, ApJ, 484, 581

Somerville R. S., et al., 2004a, ApJ, 600L, 135

Somerville R. S., Lee K., Ferguson H. C., Gardner J. P., Moustakas L. A., Giavalisco M., 2004b, ApJ, 600L, 171

Sullivan M., Hopkins A. M., Afonso J., Georgakakis A., Chan B., Cram L. E., Mobasher B., Almeida, C., 2004, ApJS, 155, 1

Yan L., et al., 2004, ApJS, 154, 75